# Magneto-optical and magnetization studies in the rare-earth orthochromites. IV. $ErCrO_3$

A. Hasson,* R. M. Hornreich,† and Y. Komet‡
*Department of Electronics, The Weizmann Institute of Science, Rehovot, Israel*

B. M. Wanklyn
*Clarendon Laboratory, Oxford, England*

I. Yaeger§
*Department of Electronics, The Weizmann Institute of Science, Rehovot, Israel*

(Received 20 January 1975)

Using combined $Er^{3+}$ absorption spectroscopy and bulk magnetization measurements, the magnetic properties of $ErCrO_3$ in the $\Gamma_1$, $\Gamma_2$, and $\Gamma_4$ phases have been studied as a function of temperature and external field. The experimental data are analyzed using a single-ion effective field model. For the $\Gamma_4$ and $\Gamma_1$ phases the most general Cr-Er and Er-Er coupling terms allowed by symmetry are considered and the canting angle of the ordered $Cr^{3+}$ spins (in the $\Gamma_4$ phase) is not constrained *a priori* to be temperature independent. It is concluded that the Cr-Er coupling is antisymmetric in nature and due mainly to Dzyaloshinsky-Moriya type exchange. For this type of interaction, the $Cr^{3+}$ canting angle is indeed temperature independent and this conclusion justifies the constant-canting-angle assumption used extensively in the literature. The Er-Er coupling is found to be of dipolar origin and it is shown that this interaction results in a significant temperature dependence of the effective splitting factor as deduced from optical-absorption measurements. For the $\Gamma_2$ phase, the data for temperatures above 20°K are interpreted in terms of a constant-canting-angle model for the Cr-Er interaction. At lower temperatures it is argued that the dipolar Er-Er coupling must also be considered.

## I. INTRODUCTION

The compound $ErCrO_3$, in conformity with other rare-earth orthochromites, crystallizes in an orthorhombically distorted perovskite structure (space group *Pbnm*) with four formula units per unit cell.[1] The exchange coupling between the $Cr^{3+}$ nearest neighbors is predominantly antiferromagnetic and these ions order magnetically at a Néel temperature of $T_N = 133\,°K$. Below this temperature and down to approximately 10 °K, $ErCrO_3$ exhibits a weak ferromagnetic moment.

The magnetic properties of $ErCrO_3$ have been extensively investigated. The experimental techniques employed include neutron diffraction,[2,3] bulk magnetization and susceptibility measurements on powders[4] and single crystals,[3,5] specific-heat studies on powders[3] and single crystals,[6] Mössbauer measurements,[7] and optical-absorption spectroscopy studies of[8,9] $Er^{3+}$ and[9,10] $Cr^{3+}$ energy levels. The results of these studies may be briefly summarized as follows: Below $T_N$ the spin structure of the $Cr^{3+}$ ions is, in the notation of Koehler *et al.*[11] and Bertaut,[12] primarily[2] $G_x$, and belongs to the $\Gamma_4$ representation. This implies that the weak ferromagnetic component of the $Cr^{3+}$ moments is in the $c$ crystallographic direction,[12] in agreement with the results of single-crystal magnetization studies.[3,5] At $T_R \simeq 10\,°K$ the $Cr^{3+}$ moments undergo a spin-reorientation-type phase transition from the $\Gamma_4(F_z)$ phase to a $G_y$ or $\Gamma_1(0)$ phase in which the ferromagnetic moment vanishes. This reorientation has been studied by magnetization,[3] specific-heat,[6] and optical studies.[8-10] Below $T_R$ the $\Gamma_4$ phase can be recovered by applying a small (1–2-kOe) external field along the $c$ crystallographic axis.[3,8,10] The third spin configuration found in the rare-earth orthochromites[13] and orthoferrites,[14] namely, $F_x G_z$ or $\Gamma_2(F_x)$ can be induced in $ErCrO_3$ by applying an external field along the $a$ crystallographic axis.[3,5,10] The critical field $H_{crit}$ required to completely reorient the $Cr^{3+}$ spins increases monotonically with decreasing temperature, gradually at first and then steeply when $T < 50\,°K$. At 20 °K, the lowest temperature reported,[5] $H_{crit} \simeq 11$ kOe.

In this paper, we present the results of extensive magnetic and magneto-optical studies of $ErCrO_3$ which complement and extend those that have been reported by other workers. In particular, we are concerned with the nature of the Cr-Er and Er-Er interactions in this compound.

In Sec. II, we first outline the various measurements performed and present the experimental results of the optical-absorption and bulk-magnetization studies. Next, in Sec. III, we analyze the experimental data for each of the three phases studied and for the spontaneous $\Gamma_4 \rightleftharpoons \Gamma_1$ phase transition at $T = T_R$. For the $\Gamma_4$ and $\Gamma_1$ phases, we take into account all types of Cr-Er and Er-Er couplings allowed by symmetry. In this analysis we do *not*

assume *a priori* that the canting angle of the $Cr^{3+}$ spin system in the $\Gamma_4$ phase is temperature independent, as was done in earlier work.[15-17] Instead, we consider the coupled $Cr^{3+}$ and $Er^{3+}$ spin systems as a single entity, with the canting angle determined by minimizing the total free energy of the system. For the $\Gamma_2$ phase, our analysis is concentrated on the temperature region above 20 °K, where the influence of the Er-Er interaction is minimal and where optical-absorption data are available. At lower temperatures, the Er-Er coupling must also be considered. Finally, in Sec. IV, the results of the experimental data analysis are summarized and our conclusions regarding the nature of the Cr-Er and Er-Er interactions are presented.

## II. EXPERIMENTAL

### A. Experimental details

Our studies were carried out on flux-grown single crystals of $ErCrO_3$. The crystallographic axes were identified by a knowledge of the symmetry and morphological features of the crystals.[1,18] For the spectroscopic measurements, selected, flux-free crystals were cut into platelets and polished down to thicknesses of 25 to 50 $\mu$m. Although platelets having (001) and (110) faces are, in principle, sufficient for measurement purposes, (100) and (010) platelets were also studied. A Jarrel-Ash 1-m grating spectrometer was used to obtain a monochromatic beam with a 0.2-Å bandwidth normally incident on the platelet. The transmitted light was detected by a photomultiplier and, after amplification, its intensity was recorded on a strip-chart reorder as a function of wave number. Linearly polarized light was used throughout. Independent absolute wave number calibrations were carried out using mercury and neon light sources of known spectral content.

Spectroscopic measurements of the absorption spectrum of $Er^{3+}$ in $ErCrO_3$ were carried out between 4.2 and 120 °K. In particular, we concentrated on the absorption lines corresponding to transitions between the lowest-lying crystal-field states of $^4I_{15/2}$ and excited crystal-field states belonging to $^4F_{9/2}$ and $^4S_{3/2}$. Since each crystal-field Kramers doublet is further split by magnetic interactions, the absorption spectra consisted of subgroups, each containing a maximum of four absorption lines. Measurements were carried out in an optical cryostat of our own design in which the sample was cooled by a stream of helium vapor. Constant temperatures were maintained with the help of a temperature controller operated by a magnetic valve. External fields of up to 24 kOe were obtained by positioning the cryostat between the poles of an electromagnet.

Bulk magnetization and susceptibility measurements were performed using both a motor-driven vibrating sample magnetometer and pulsed-field techniques. The measurements were carried out in the 4.2–140 °K range. The reported results were compiled from (a) magnetization curves versus temperature recorded at various fixed magnetic fields while cooling the sample and (b) curves of magnetization versus applied field recorded at fixed temperatures. The cooling and temperature control system used was similar to that employed in the optical studies. Full experimental details are given elsewhere.[19-21]

### B. Experimental results

In Figs. 1 and 2 we show typical absorption spectra corresponding to $^4I_{15/2} \rightarrow {}^4F_{9/2}$ and $^4I_{15/2} \rightarrow {}^4S_{3/2}$ transitions, respectively. Each figure shows spectra taken above and below the reorientation temperature $T_R$ in zero external field. The spectra of Fig. 1 were taken on a (010) platelet with $\vec{E} \parallel \vec{c}$ and $\vec{E} \parallel \vec{a}$ while those of Fig. 2 were taken on a (110) platelet with $\vec{E} \parallel \vec{c}$ and $\vec{E} \perp \vec{c}$. The notation is that of Faulhaber *et al.*,[22] wherein the crystal-field levels of the ground term are labeled with Roman numbers (I, II, ...) and those of the excited terms with lower-case letters ($a, b, \ldots$) starting with $a$ for the level with lowest energy. The recorded linewidths at 77 °K varied between 4 and 10 $cm^{-1}$. At 4.2 °K, typical values were from 2 to 5 $cm^{-1}$. [The latter refer to the transitions I$a$ to I$e$ ($a$-$e$ of $^4F_{9/2}$), as higher-lying doublets of $^4I_{15/2}$ are essentially unoccupied at this temperature.] The crystal-field levels studied by us are

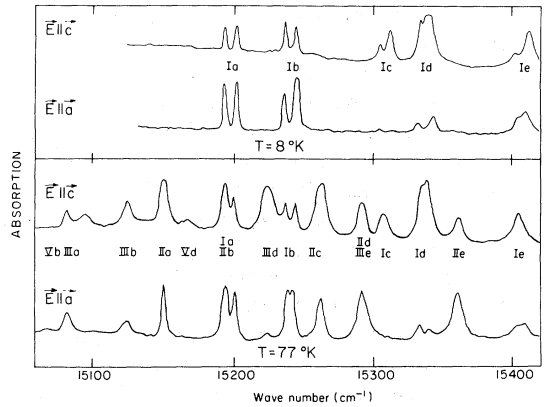


FIG. 1. Optical-absorption spectra of $Er^{3+}$ in $ErCrO_3$ for polarizations parallel to the $c$ and $a$ crystallographic axis. (I, II, III, V refer to the lowest-lying Kramers doublets of the $^4I_{15/2}$ ground state, and $a$, $b$, $c$, $d$, $e$ to the Kramers doublets of the $^4F_{9/2}$ excited state.)

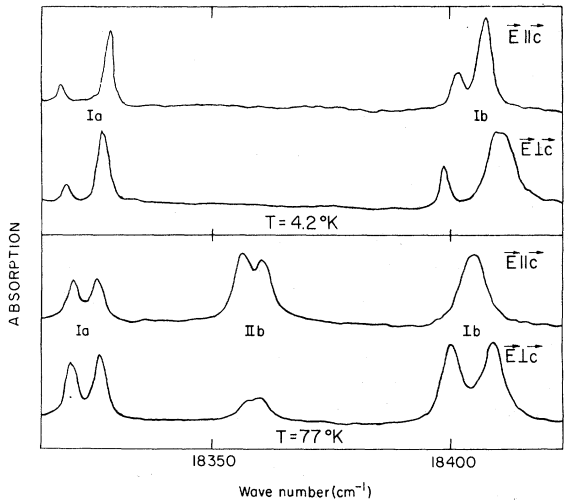


FIG. 2. Optical-absorption spectra of $Er^{3+}$ in $ErCrO_3$ for polarization parallel and perpendicular to the $c$ crystallographic axis. (I, II refer to the lowest-lying Kramers doublets of the $^4I_{15/2}$ ground state, and $a$, $b$ to the Kramers doublets of the $^4S_{3/2}$ excited state.)

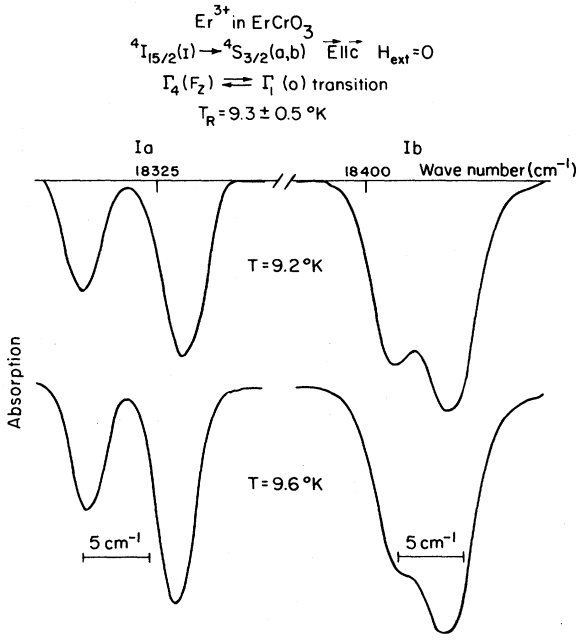


FIG. 3. Optical-absorption spectra of $Er^{3+}$ in $ErCrO_3$ immediately above and below the spin-reorientation temperature $T_R$ obtained with $c$-axis polarized light. (I refers to the lowest-lying Kramers doublet of the $^4I_{15/2}$ ground state, and $a$, $b$, to the Kramers doublets of the $^4S_{3/2}$ excited state.)

listed in Table I.

The spin-reorientation transition was found to occur at $T_R = 9.3 \pm 0.5$ °K. The transition region was less than 0.1 °K in width. This is in agreement with results reported by other workers.[3,6,8,10] An example of absorption spectra recorded at temperatures immediately above and below $T_R$ is presented in Fig. 3.

Spectra were also recorded with an external field applied along the $c$ or $a$ crystallographic axis. Typical results are shown in Figs. 4 and 5. Those

TABLE I. Some crystal-field levels of $Er^{3+}$ in $ErCrO_3$.

| Group | Kramers doublet label | Energy ($cm^{-1}$) |
|---|---|---|
| $^4I_{15/2}$ | I | 0 |
| | II | 46 ± 1 |
| | III | 114 ± 2 |
| | IV [a] | ... |
| | V [a] | 173 ± 3 |
| $^4F_{9/2}$ | $a$ | 15 197 ± 3 |
| | $b$ | 15 241 ± 3 |
| | $c$ | 15 308 ± 3 |
| | $d$ | 15 337 ± 3 |
| | $e$ | 15 407 ± 3 |
| $^4S_{3/2}$ | $a$ | 18 324 ± 3 |
| | $b$ | 18 405 ± 3 |

[a] The level at 173 $cm^{-1}$ was assigned to doublet V by comparing the level structure of $ErCrO_3$ ($^4I_{15/2}$) with that of $ErFeO_3$ ($^4I_{15/2}$) (see Table IV and Ref. 41).

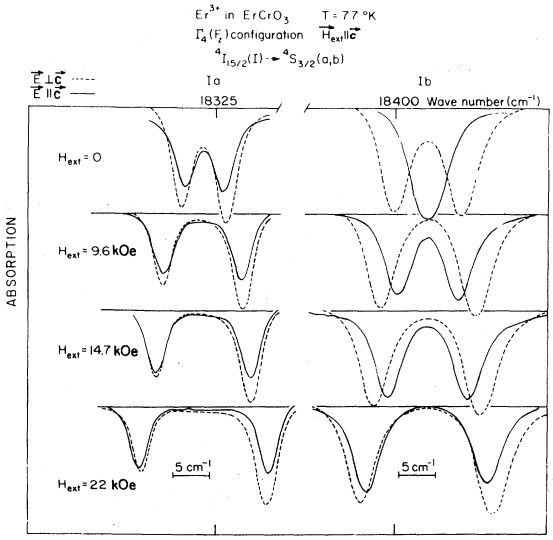


FIG. 4. Optical-absorption spectra of $Er^{3+}$ in $ErCrO_3$ for polarizations parallel and perpendicular to the $c$ crystallographic axis in a magnetic field applied parallel to $c$. (I refers to the lowest-lying Kramers doublet of the $^4I_{15/2}$ ground state, and $a$, $b$, to the Kramers doublet of the $^4S_{3/2}$ excited state.

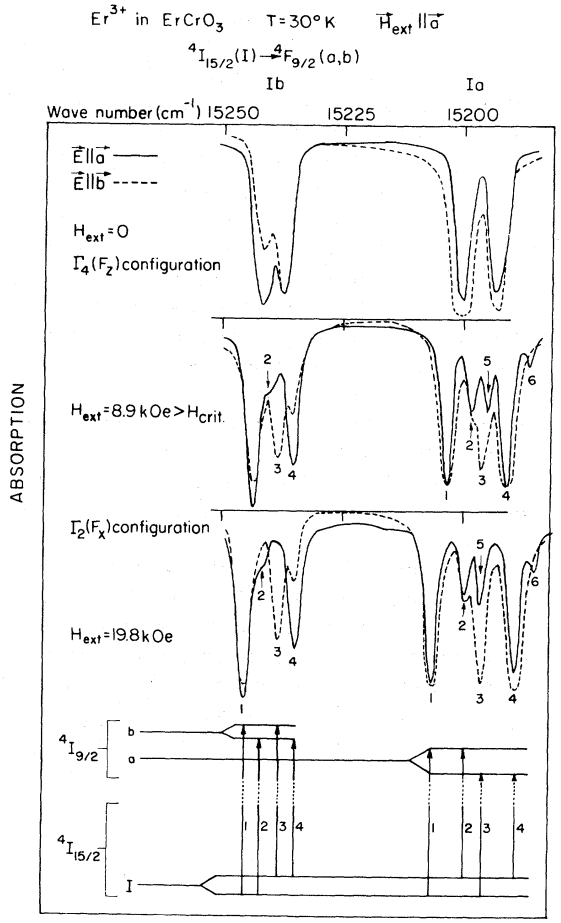


FIG. 5. Optical-absorption spectra of $Er^{3+}$ in $ErCrO_3$ for polarizations parallel to the *a* and *b* crystallographic axis in a magnetic field applied parallel to *a*. (I refers to the lowest-lying Kramers doublet of the $^4I_{15/2}$ ground state, and *a*, *b* to the Kramers doublets of the $^4F_{9/2}$ excited state.)

of Fig. 4 were taken on a (110) platelet at 77 °K with polarization $\vec{E}\|\vec{c}$ and $\vec{E}\perp\vec{c}$, and $\vec{H}_{ext}\|\vec{c}$. The absorption lines correspond to the transitions $^4I_{15/2}(I)\rightarrow{}^4S_{3/2}(a,b)$. The spectra of Fig. 5 were taken on a (001) platelet at 30 °K with polarization $\vec{E}\|\vec{a}$ and $\vec{E}\|\vec{b}$, and $\vec{H}_{ext}\|\vec{a}$. The absorption lines correspond to the transitions $^4I_{15/2}(I)\rightarrow{}^4F_{9/2}(a,b)$, as shown schematically in the figure.

In $ErCrO_3$, the $Er^{3+}$ ions are in sites having the symmetry $C_s(m)$. For ions with an odd number of electrons located at sites having such low symmetry, a $^{2S+1}L_J$ level is split by the crystalline field into $\frac{1}{2}(2J+1)$ Kramers doublets. These degenerate pairs of crystal-field states can be labeled with the representations $A_3$, $A_4$ of the site group.[23] The selection rules for electric and magnetic dipole transitions between these states are given in Table II.[21,24] The $Er^{3+}$ crystal-field states are of course modified and shifted when magnetic fields are present. In particular, the influence of the ordered $Cr^{3+}$ spin system below $T_N$ can be represented, in the molecular-field approximation, by an effective magnetic field acting at the $Er^{3+}$ sites. For spin structure belonging to either $\Gamma_4$ or $\Gamma_1$, this effective field is along the *c* axis, and the selection rules given in Table II are applicable. In the presence of an applied field $\vec{H}_{ext}\|\vec{c}$ they still remain valid, but not when $\vec{H}_{ext}\perp\vec{c}$.

Thus, for the polarized-light spectra of Figs. 1–3, we expect at most two spectral lines from a given subgroup of four to appear for a given polarization, assuming that either an electric or magnetic dipole transition mechanism is dominant. Since spectra taken with $\vec{E}\perp\vec{c}$, $\vec{H}\|\vec{c}$ [(110) platelet] and spectra taken with $\vec{E}\|\vec{a}$, $\vec{H}\|\vec{b}$ [(001) platelet] were identical, it follows that all the observed absorption lines are due to electric dipole transitions. Following this assignment, the separation of ground- and excited-state Zeeman splitting is straightforward.[8,21] By comparing the separated $^4I_{15/2}(I)\rightarrow{}^4S_{3/2}$ and $^4I_{15/2}(I)\rightarrow{}^4F_{9/2}$ Zeeman splittings, an unambigous identification of the ground doublet splitting $\Delta E$ could be made. The results for $\Delta E(T)$ for the $\Gamma_4$ and $\Gamma_1$ phases in zero external field are presented in Fig. 6. They are essentially the same as those of Courths *et al.*[8] Also given are the values of $\Delta E(T)$ for the $\Gamma_4$ phase for $T<T_R$, obtained by extrapolating the appropriate $\Delta E$ versus applied field curves to zero external field.

In the $\Gamma_2$ phase, the selection rules of Table II are no longer valid.[24,25] Thus, as seen in Fig. 5, there occurs a "leak through" of those spectral lines forbidden in zero external field for a given polarization. This did not cause any difficulties when interpreting the spectral lines, as the various transitions could be identified by comparison with the $\Gamma_4$ phase spectra. The experimental data, based on the $^4I_{15/2}(I)\rightarrow{}^4F_{9/2}(a, b, d, e)$ transitions, are summarized in Fig. 7. Data are given only for

TABLE II. Selection rules for electric and magnetic dipole transitions in the group $C_s(m)$. The mirror plane is perpendicular to *z*. $\vec{E}$ and $\vec{H}$ refer to the electric and magnetic field vectors of the radiation inducing the transition.

| Transition | $A_3\leftrightarrow A_3$, $A_4\leftrightarrow A_4$ | $A_3\leftrightarrow A_4$ |
|---|---|---|
| Electric dipole allowed | $\vec{E}\perp\vec{z}$ | $\vec{E}\|\vec{z}$ |
| Magnetic dipole allowed | $\vec{H}\|\vec{z}$ | $\vec{H}\perp\vec{z}$ |

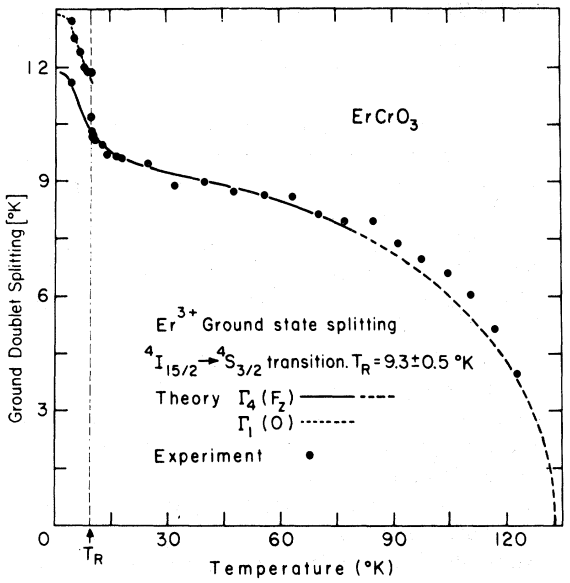


FIG. 6. Temperature dependence of the ground-doublet splitting of $Er^{3+}$ in $ErCrO_3$ in the $\Gamma_4(F_z)$ and $\Gamma_1(O)$ phases. (Experimental points and calculated fit are shown. Extrapolation of the calculated curve outside the fits region is indicated by a dashed line.)

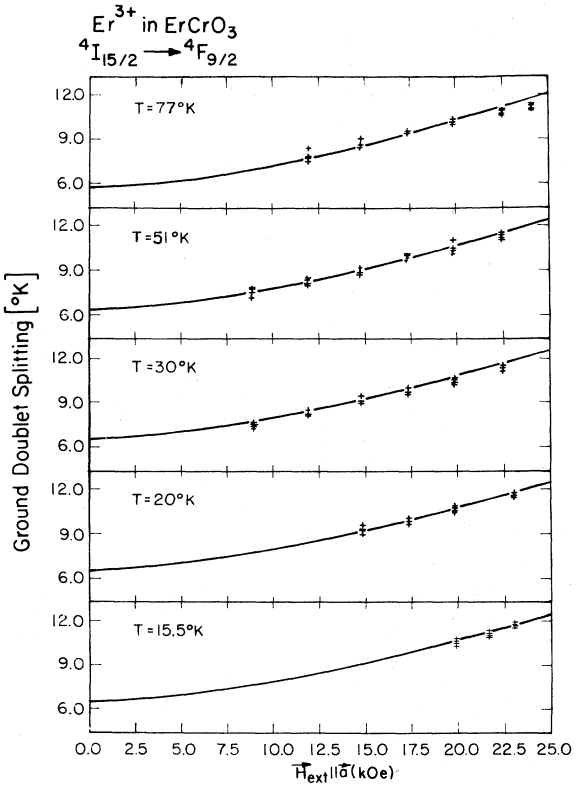


FIG. 7. Field dependence of the ground doublet splitting of $Er^{3+}$ in $ErCrO_3$ in the $\Gamma_2(F_x)$ phase at various temperatures. (The experimental points and calculated fit are shown.)

$H > H_{crit}$, as the $\Gamma_2$ phase exists only in this field region.

Turning to the bulk-magnetization studies, we present in Fig. 8 the magnetization of $ErCrO_3$ in its $\Gamma_4$ phase below $T_N = 133\,°K$ and down to 4.2 °K. For $T_N > T > T_R$ this curve is identical with the spontaneous magnetization[3] which vanishes for $T \leq T_R$. Below $T_R$ the magnetization data given were obtained by applying a $c$-direction field to restore the $\Gamma_4$ phase and then extrapolating the resulting magnetization versus applied field curve to zero applied field. In Fig. 9, the principal magnetic susceptibility in the $c$ direction is given. For $T < T_R$ the susceptibility was obtained from the slope of the magnetization versus field curve in the $\Gamma_4$ phase. This method was adopted in order to avoid the rotational contribution to the susceptibility when the $Cr^{3+}$ moments[26] rotate from the $\Gamma_1$ to the $\Gamma_4$ phase.

The magnetization data obtained for $\Gamma_2$ phase $ErCrO_3$ are presented in Figs. 10–12. First, in Fig. 10, the threshold field $H_{crit}$ required to induce the $\Gamma_2$ phase at a given temperature is given. This is an extension of earlier results[3,5] down to 4.2 °K. In Figs. 11 and 12, are shown the extrapolated zero-field magnetization and high-field susceptibility. These were obtained from the $H > H_{crit}$ magnetization versus applied field curves in the same manner as described previously for the $\Gamma_4$ phase $T < T_R$ data.

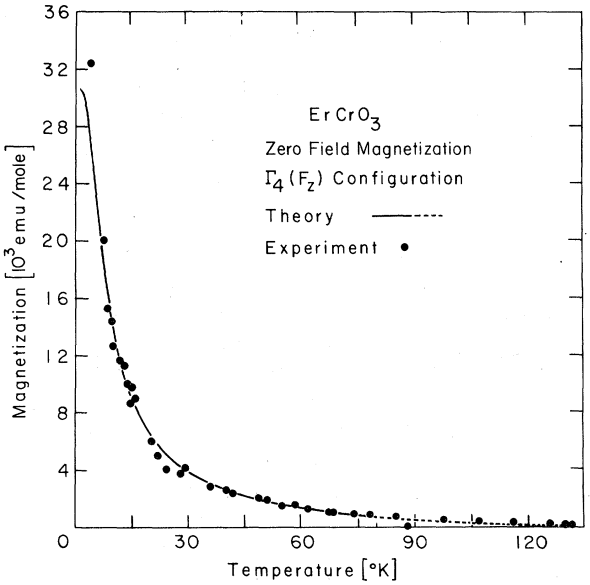


FIG. 8. Temperature dependence of the magnetization of $ErCrO_3$ in the $\Gamma_4(F_z)$ phase. The experimental data were corrected for demagnetization effects. (The experimental points and calculated fit are shown. The extrapolation of the calculated curve outside the fit region is indicated by a dashed line.)

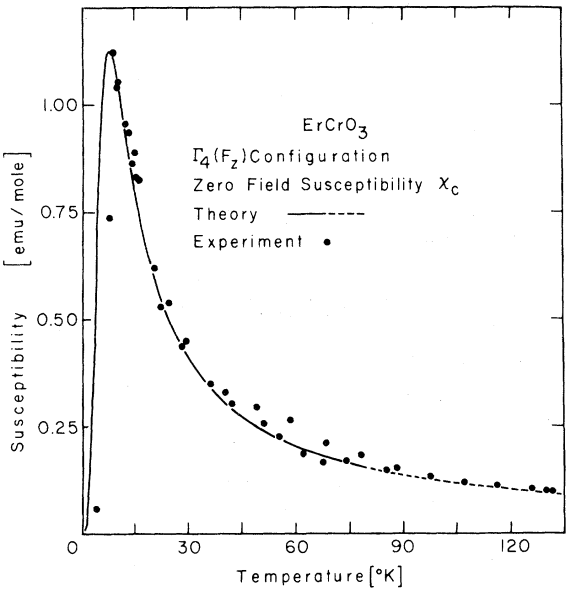


FIG. 9. Temperature dependence of the $c$-axis susceptibility of $ErCrO_3$ in the $\Gamma_4(F_z)$ phase. The experimental points shown for $T < T_R$ were obtained by extrapolating the magnetization versus field curves to zero applied field, and all data were corrected for demagnetization effects. (The experimental points and calculated fit are shown. The extrapolation of the calculated curve outside the fit region is indicated by a dashed line.)

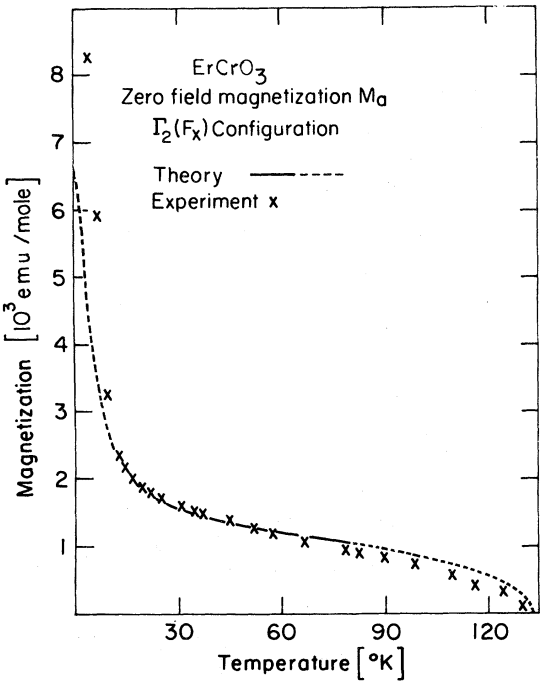


FIG. 11. Temperature dependence of the magnetization of $ErCrO_3$ in the $\Gamma_2(F_x)$ phase. The experimental points shown were obtained by extrapolating the magnetization versus field curves to zero applied field and corrected for demagnetization effects. (The experimental points and calculated fit are shown. The extrapolation of the calculated curve outside the fit region is indicated by a dashed line.)

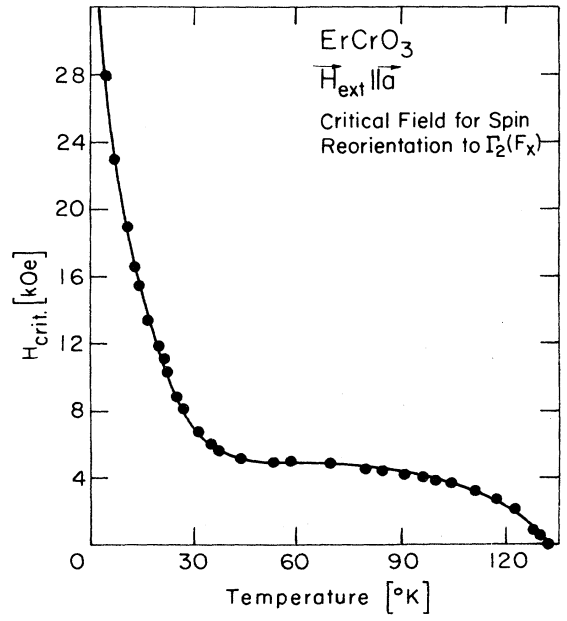


FIG. 10. Temperature dependence of the threshold field $H_{crit}$ required to induce the $\Gamma_2(F_x)$ phase. The experimental data were corrected for demagnetization effects.

## III. ANALYSIS

### A. $\Gamma_4$ phase

As noted earlier, the $^{2S+1}L_J$ levels of $Er^{3+}$ are split into Kramers doublets by the crystalline field. We see from Table I that the splitting between the two lowest-lying doublets is 46 $cm^{-1}$ or 66 °K. Thus, at sufficiently low temperatures ($T < 50$ °K), only the two states comprising the lowest-lying doublet will be significantly occupied. We shall show that the main features of the $\Gamma_4$ phase optical-absorption and bulk-magnetization data can be understood in terms of the polarization of the electrons occupying the $Er^{3+}$ ground doublet by the effective fields of the $Cr^{3+}$ and $Er^{3+}$ spin systems.

Between $T_N = 133$ °K and $T_R$, the $Cr^{3+}$ spins are in an $F_xG_z$ structure belonging to $\Gamma_4$. As shown by Bertaut,[12] this structure couples to, and therefore can induce, an $f_z$ mode for the $Er^{3+}$ spins. Thus the total effective field exerted by the ordered $Cr^{3+}$ and polarized $Er^{3+}$ spin systems upon a given $Er^{3+}$ moment will lie along the $c$ crystallographic axis. This fixed direction for the effective field greatly

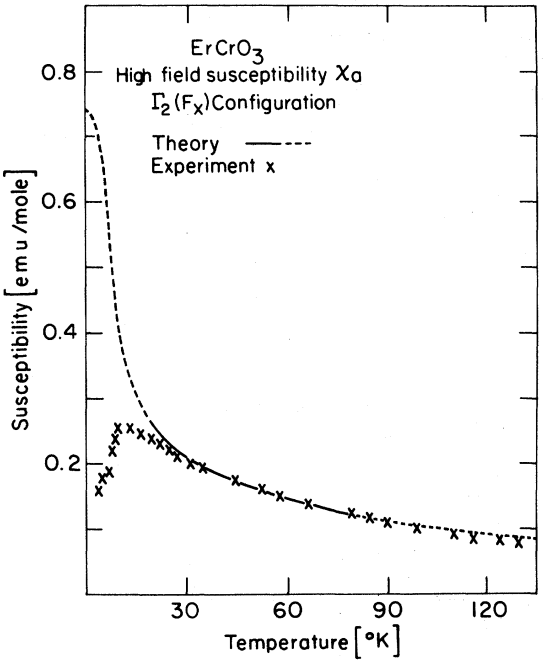


FIG. 12. Temperature dependence of the $a$-axis susceptibility in the high-field $\Gamma_2(F_x)$ phase. The experimental points were corrected for demagnetization effects. (The experimental points and calculated fit are shown. The extrapolation of the calculated curve outside the fit region is indicated by a dashed line.)

simplifies the analysis and permits us to dispense with the usual *a priori* assumption that the canting angle, i.e., the angle between the $Cr^{3+}$ sublattice moment and the antiferromagnetic axis, is temperature independent. As we shall show, depending upon the nature of the $Cr^{3+}$-$Er^{3+}$ coupling, $\alpha$ can indeed vary with the temperature. This was first pointed out, to our knowledge, by Beaulieu.[27]

Using the subscript $\alpha$ to designate the $\Gamma_4$ phase, the spin Hamiltonian of our system

$$\mathcal{H}_\alpha = \mathcal{H}_\alpha^{Cr-Cr} + \mathcal{H}_\alpha^{Er-Er} + \mathcal{H}_\alpha^{Cr-Er} \tag{1}$$

is written as a sum of three terms describing, respectively, the interactions between $Cr^{3+}$ spins, between $Er^{3+}$ spins, and between $Cr^{3+}$ and $Er^{3+}$ spins. We introduce a coordinate system $x$, $y$, $z$ parallel to the orthorhombic crystallographic axes. Considering first $\mathcal{H}_\alpha^{Cr-Cr}$, a two-sublattice description for the $Cr^{3+}$ spin system will be sufficient for our study.[21] In the $\Gamma_4$ phase the spins lie essentially in the plus and minus $x$ directions, and the appropriate Hamiltonian is[28]

$$\begin{aligned}\mathcal{H}_\alpha^{Cr-Cr} = &-(\tfrac{1}{2}Ng_c\mu_B)^2[-\lambda(S_{1x}S_{2x}+S_{1z}S_{2z}) \\ &+D(S_{1x}S_{2z}-S_{1z}S_{2x})+\tfrac{1}{2}K(S_{1x}^2+S_{2x}^2)] \\ &-\tfrac{1}{2}g_c\mu_B NH_c(S_{1z}+S_{2z}),\end{aligned} \tag{2}$$

where $\vec{S}_1$, $\vec{S}_2$ are representative $Cr^{3+}$ spins in the plus and minus sublattices, respectively, $g_c$ is the $z$-axis $g$ factor, $\mu_B$ is the Bohr magneton, and $N$ is the number of $Cr^{3+}$ spins per mole of $ErCrO_3$ (Avogadro's number). For $Cr^{3+}$ ions, $S=\frac{3}{2}$ and $g_c=2$. The first and second terms denote symmetric (Heisenberg) and antisymmetric (Dzyaloshinsky-Moriya) exchange, the third, a uniaxial anisotropy which fixes (for $K<0$) the crystallographic $a$ axis as the easy direction for each spin sublattice, and the last, the coupling of the spins to an external field $H_c$ applied along the $z$ axis. The coefficients $\lambda$, $D$, and $K$ are interaction constants. For space group $Pbnm$, the Dzyaloshinsky vector $\vec{D}$ is along the $y$ direction,[12] and all moments lie in the $xz$ plane in the $\Gamma_4$ phase. We assume, in conformity with previous results for the rare-earth orthoferrites[29-31] and orthochromites,[20,30] that the $xz$-plane anisotropy term[29] allowed by symmetry is negligible compared with the antisymmetric exchange term.

Turning to $\mathcal{H}_\alpha^{Er-Er}$, the most general expression allowed by symmetry is[21,24]

$$\begin{aligned}\mathcal{H}_\alpha^{Er-Er} = &-(\tfrac{1}{2}Ng_z\mu_B)^2\Big(\tfrac{1}{2}G_1\sum_i J_{iz}^2+G_2(J_{1z}J_{2z}+J_{3z}J_{4z}) \\ &+G_3(J_{2z}J_{4z}+J_{1z}J_{3z})+G_4(J_{2z}J_{3z}+J_{1z}J_{4z})\Big) \\ &-\tfrac{1}{4}g_z\mu_B NH_c\sum_i J_{iz},\end{aligned} \tag{3}$$

where $J_{iz}$ is the $z$ component of the effective spin operator at site $i$ and the summation is over the four $Er^{3+}$ sites per unit cell. For an isolated Kramers doublet, $J=\frac{1}{2}$. The $G_i$ are coupling coefficients and $g_z$ is the $z$-axis effective splitting factor of the $Er^{3+}$ ground doublet.

Finally, $\mathcal{H}_\alpha^{Cr-Er}$ is given by[21,24]

$$\begin{aligned}\mathcal{H}_\alpha^{Cr-Er} = &-(\tfrac{1}{4}N\mu_B)^2 g_c g_z \\ &\sum_i J_{iz}[D_1(S_{1z}+S_{2z})+D_2(S_{1x}-S_{2x})],\end{aligned} \tag{4}$$

where $D_1$ and $D_2$ are coupling coefficients denoting the magnitudes of the symmetric and antisymmetric parts of the Cr-Er interaction, respectively.

To calculate the magnetic properties of the coupled spin system described by (1), it is useful to work with the Gibbs free-energy functional. It is defined as

$$\mathcal{F}(M,\vec{H},\vec{T}) \equiv A(\vec{M},T)-\vec{M}\cdot\vec{H}, \tag{5}$$

where $A$, the magnetic analog of the Helmholtz free energy, is given by

$$A = U - T\sigma = \epsilon + \vec{M}\cdot\vec{H} - T\sigma = \langle\mathcal{H}\rangle + \vec{M}\cdot\vec{H} - T\sigma. \tag{6}$$

Here $U(\vec{M},\sigma)$ and $\epsilon(\vec{H},\sigma)$ are the internal energy and magnetic enthalpy of the system,[32] $\vec{M}$ is the magnetization, $T$ the temperature, and $\sigma$ the total entropy of the system. $\vec{H}$, as before, is an external field, and $\langle\ \rangle$ denotes an average over a canonical ensemble. At thermodynamic equilibrium, $\vec{H}=\nabla_{\vec{M}}A|_T$, from which it follows that the equilibrium value $\vec{M}(\vec{H},T)$ can be determined implicitly from the condition

$$\nabla_{\vec{M}}\mathcal{F}_{\vec{H},T}=0\ . \tag{7}$$

To calculate $\langle\mathcal{K}_\alpha\rangle$ for the $\Gamma_4$ phase, we use

$$\begin{aligned}&\langle S_{1x}\rangle=-\langle S_{2x}\rangle=\langle S\rangle\cos\alpha\ ,\\ &\langle S_{1z}\rangle=\langle S_{2z}\rangle=\langle S\rangle\sin\alpha\ ,\\ &\langle J_{iz}\rangle=\langle J\rangle\ ,\quad i=1,\ldots,4,\end{aligned} \tag{8}$$

and introduce

$$\mu=\tfrac{1}{2}g_c\mu_B N\langle S\rangle\ ,\quad m_c=g_z\mu_B N\langle J\rangle\ . \tag{9}$$

Here $\alpha$ is the angle between the $Cr^{3+}$ sublattice moment and the $a$ axis, $\mu$ is the $Cr^{3+}$ sublattice moment, and $m_c$ is the total $Er^{3+}$ ferromagnetic moment. Using (8) and (9) we obtain, in the molecular-field approximation,

$$\begin{aligned}\langle\mathcal{K}_\alpha\rangle=&-\lambda\mu^2\cos2\alpha-D\mu^2\sin2\alpha-K(T)\mu^2\cos^2\alpha\\ &-2\mu H_c\sin\alpha\\ &-\tfrac{1}{2}G_\alpha m_c^2-H_c m_c-D_1\mu m_c\sin\alpha-D_2\mu m_c\cos\alpha,\end{aligned} \tag{10}$$

where

$$\begin{aligned}&K(T)=K\left[\langle S^2\rangle-\tfrac{1}{3}S(S+1)\right]/\langle S\rangle^2\ ,\\ &G_\alpha=\sum_i G_i\ .\end{aligned} \tag{11}$$

In a molecular-field framework, $\langle S\rangle$ and $\langle J\rangle$ are determined by the magnitudes of the total effective fields $H_\alpha^{Cr}$, $H_\alpha^{Er}$ acting on a given $Cr^{3+}$ or $Er^{3+}$ spin according to the relations[33]

$$\begin{aligned}&\langle S\rangle/S=B_S(g_c\mu_B SH_\alpha^{Cr}/k_BT)\ ,\\ &\langle J\rangle/J=B_J(g_z\mu_B JH_\alpha^{Er}/k_BT)\ .\end{aligned} \tag{12}$$

Further, the Cr and Er single-spin entropies $\sigma_S$, $\sigma_J$ are related to the respective spin averages by[33]

$$\begin{aligned}&\frac{\partial\sigma_S}{\partial\langle S\rangle}=-\frac{k_B}{S}B_S^{-1}\frac{\langle S\rangle}{S}=-\frac{g_c\mu_B H_\alpha^{Cr}}{T}\ ,\\ &\frac{\partial\sigma_J}{\partial\langle J\rangle}=-\frac{k_B}{J}B_J^{-1}\frac{\langle J\rangle}{J}=-\frac{g_z\mu_B H_\alpha^{Er}}{T}\ ,\end{aligned} \tag{13}$$

and

$$\sigma=N(\sigma_S+\sigma_J)\ . \tag{14}$$

Here $B_S$, $B_J$ and $B_S^{-1}$, $B_J^{-1}$ are the usual and inverse Brillouin functions, respectively, and $k_B$ is Boltzmann's constant.

Equations (5)–(7), (10), and (12)–(14) suffice to determine all the thermodynamic properties of the system. We proceed by noting that (7) is equivalent to

$$\begin{aligned}\left.\frac{\partial\mathcal{F}}{\partial\alpha}\right|_{T,H_c,\langle S\rangle,\langle J\rangle}&=\left.\frac{\partial\mathcal{F}}{\partial\langle S\rangle}\right|_{T,H_c,\alpha,\langle J\rangle}\\ &=\left.\frac{\partial\mathcal{F}}{\partial\langle J\rangle}\right|_{T,H_c,\alpha,\langle S\rangle}=0.\end{aligned} \tag{15}$$

The entropy $\sigma$ is independent of $\alpha$, thus the first part of (15) reduces to

$$\frac{\partial\langle\mathcal{K}_\alpha\rangle}{\partial\alpha}=0\ . \tag{16}$$

For $\alpha\ll1$, (10) and (16) yield

$$\alpha=\frac{D+D_1m_c/2\mu+H_c/\mu}{2\lambda+K(T)+D_2m_c/2\mu}\simeq\frac{D+D_1m_c/2\mu+H_c/\mu}{2\lambda}\ . \tag{17}$$

The right-hand expression in (17) follows as $K(T)\mu$ and $\frac{1}{2}D_2m_c$, the Cr anisotropy and Cr-Er antisymmetric interaction fields, respectively, are both at least two orders of magnitude smaller than the Cr-Cr interaction field $\lambda\mu$ for the case of $ErCrO_3$. The final two equilibrium conditions in (15), together with (13) and (14) give the usual effective field relations

$$\begin{aligned}&H_\alpha^{Cr}=-\frac{1}{g_c\mu_B N}\frac{\partial\langle\mathcal{K}_\alpha\rangle}{\partial\langle S\rangle}=-\frac{1}{2}\frac{\partial\langle\mathcal{K}_\alpha\rangle}{\partial\mu}\ ,\\ &H_\alpha^{Er}=-\frac{1}{g_z\mu_B N}\frac{\partial\langle\mathcal{K}_\alpha\rangle}{\partial\langle J\rangle}=-\frac{\partial\langle\mathcal{K}_\alpha\rangle}{\partial m_c}\ .\end{aligned} \tag{18}$$

Using $B_{1/2}(x)=\tanh x$, the total spontaneous moment of $ErCrO_3$ when only the lowest-lying $Er^{3+}$ Kramers doublet is significantly occupied is given by

$$M_c(H_c,T)=2\mu\alpha+m_c=2\mu\alpha+\tfrac{1}{2}Ng_z\mu_B\tanh(\Delta E_\alpha/2k_BT), \tag{19}$$

where

$$\Delta E_\alpha(H_c,T)=g_z\mu_B H_\alpha^{Er} \tag{20}$$

is the splitting of the lowest-lying Kramers doublet in the $\Gamma_4$ phase. The $c$ axis susceptibility is given by

$$\begin{aligned}\chi_c(T)=\frac{\partial M_c}{\partial H_c}&=2\mu\frac{\partial\alpha}{\partial H_c}+\chi_0\\ &=2\mu\left(\frac{\partial\alpha}{\partial H_c}\right)+\frac{Ng_z^2\mu_B^2}{4k_BT}\left(\frac{\partial H_\alpha^{Er}}{\partial H_c}\right)\operatorname{sech}^2\left(\frac{\Delta E_\alpha}{2k_BT}\right).\end{aligned} \tag{21}$$

All derivatives in (21) are taken at constant $T$ and evaluated at $H_c = 0$. Note that we have implicitly assumed that $\mu$ is field independent; this is justified at low temperatures ($T/T_N \leq 0.4$), where the $Cr^{3+}$ sublattice moment is essentially saturated. From (17) we have

$$\frac{\partial \alpha}{\partial H_c} = \frac{1}{2\lambda\mu} + \frac{D_1}{4\lambda\mu}\chi_0 \tag{22}$$

and, using (10), (17), (18), and (22), we obtain

$$H_\alpha^{\mathrm{Er}} = [G_\alpha m_c + \mu(D_1 \sin\alpha + D_2 \cos\alpha)] + H_c , \tag{23a}$$

$$\frac{\partial H_\alpha^{\mathrm{Er}}}{\partial H_c} = 1 + \frac{D_1}{2\lambda} + \left(G_\alpha + \frac{D_1^2}{4\lambda}\right)\chi_0 . \tag{23b}$$

In arriving at (23), we have assumed that $D_2\alpha/2\lambda$ and $D_1 D_2 (\partial m_c/\partial H_c)/4\lambda$ are negligible in comparison with the quantities remaining in the right-hand expressions. This is essentially the same approximation made earlier in (17). Combining (19)–(23) gives, for zero applied field, the results

$$\Delta E_\alpha(T) = g_z' \mu_B (D_1\alpha_0 + D_2)'\mu + \tfrac{1}{2} N (g_z')^2 \mu_B^2 G_\alpha' \tanh\left(\frac{\Delta E_\alpha(T)}{2k_B T}\right) , \tag{24a}$$

$$M_c(T) = 2\mu\alpha_0 + \tfrac{1}{2} N g_z' \mu_B \tanh\left(\frac{\Delta E_\alpha(T)}{2k_B T}\right) , \tag{24b}$$

$$\chi_c(T) = \frac{1}{\lambda} + \frac{N(g_z')^2\mu_B^2}{4k_B T}\,\mathrm{sech}^2\left(\frac{\Delta E_\alpha(T)}{2k_B T}\right) \times \left[1 - \frac{N(g_z')^2\mu_B^2 G_\alpha'}{4k_B T}\,\mathrm{sech}^2\left(\frac{\Delta E_\alpha(T)}{2k_B T}\right)\right]^{-1} , \tag{24c}$$

where

$$\alpha_0 = D/2\lambda , \tag{25}$$

$$g_z' = g_z(1 + D_1/2\lambda) , \tag{26a}$$

$$(D_1\alpha_0 + D_2)' = \frac{D_1\alpha_0 + D_2}{1 + D_1/2\lambda} , \tag{26b}$$

$$G_\alpha' = \frac{G_\alpha + D_1^2/4\lambda}{(1 + D_1/2\lambda)^2} . \tag{26c}$$

From a self-consistent solution of (24) we can obtain the three quantities of interest, namely, the splitting of the ground doublet $\Delta E_\alpha(T)$, the spontaneous magnetization $M_c(T)$, and the $c$-axis susceptibility $\chi_c(T)$. The $Cr^{3+}$ sublattice moment $\mu$, which appears in (24a), is determined independently from

$$\mu = \tfrac{1}{2} g_c \mu_B N S B_S(g_c \mu_B S \lambda \mu / k_B T) . \tag{27a}$$

In (27a) the other interaction fields have been neglected in comparison with the dominant Cr-Cr Heisenberg exchange coupling. The exchange constant $\lambda$ was found from the usual molecular-field expression for the transition point[28]

$$T_N = N g_c^2 \mu_B^2 S(S+1)\lambda/6k_B \tag{27b}$$

to be $\lambda = 142$ mole Oe/emu. Note that an accurate value of $\lambda$ is not critical to our study.

The most important consequence of the general derivation we have presented is given by (26). We have seen earlier, in (17), that the Cr-Er coupling can result in a change in the canting angle due to the "back reaction" of the polarized $Er^{3+}$ spins on the $Cr^{3+}$ spin system. This leads, in (24), to the replacement of $g_z$, $(D_1\alpha_0 + D_2)$, and $G_\alpha$ by their "renormalized" counterparts. Further, we see from (26) that the renormalization depends only on the symmetric part of the Cr-Er interaction; if the interaction is predominantly antisymmetric, the three renormalized quantities become identical with their unprimed counterparts. We also see that the functional form of (24) is unaffected by the "back-reaction" effect. Thus a successful fit of (24) to the experimental data cannot, by itself, allow us to draw any conclusions regarding the nature of the Cr-Er interaction.

It is an accepted technique to determine the splitting factor in a given direction by extrapolating the slope $(\partial\Delta E/\partial H)_T$ to zero applied field. From (20), (23), and (24) the effective optical-splitting factor $g_z''$ in the $\Gamma_4$ phase is thus given by

$$g_z'' = \frac{1}{\mu_B}\left(\frac{\partial \Delta E_\alpha}{\partial H_c}\right)_T = g_z'[1 + G_\alpha' \chi^{\mathrm{Er}}(T)] , \tag{28a}$$

where

$$\chi^{\mathrm{Er}}(T) = \chi_c(T) - 1/\lambda . \tag{28b}$$

We see that $g_z''$ is not equal to either $g_z$ or $g_z'$. It is instead a temperature-dependent quantity.

Values for the parameters $\alpha_0$, $g_z'$, $(D_1\alpha_0 + D_2)'$, and $G_\alpha'$ were initially determined by fitting the experimental data of Figs. 6, 8, and 9 to the expression given in (24) in the temperature range $4.2 < T < 80$ °K. A computerized least-squares technique was employed to fit all three sets of data simultaneously. A best fit was obtained with the following values:

$$\begin{aligned} &\alpha_0 = -60 \pm 60 \text{ mrad}, \\ &g_z' = 11.3 \pm 0.3, \\ &(D_1\alpha_0 + D_2)' = 1.4 \pm 0.1 \text{ mole Oe/emu}, \\ &G_\alpha' = 0.13 \pm 0.05 \text{ mole Oe/emu}. \end{aligned} \tag{29a}$$

The errors quoted above and henceforth are statistical and indicate two standard deviations.

Using (24) and (29a), the ground doublet splitting, magnetization, and $c$-axis susceptibility were cal-

culated for $4.2 < T < T_N$. The calculated curves are shown in Figs. 6, 8, and 9. Generally speaking, the fit is excellent over the entire temperature range, indicating that doublet II, centered at 66 °K, does not contribute significantly to $M_c$ and $\chi_c$.

In order to reduce the statistical errors given in (29a), the data were further analyzed in three alternative ways. Thus, at temperatures $T \geq \Delta E_\alpha(T)/k_B$, the set of equations in (24) can be combined to give[29,34]

$$M_c(T)/\mu \simeq 2\alpha_0[1 + (D_1\alpha_0 + D_2)'\chi^{\mathrm{Er}}/2\alpha_0] . \quad (30)$$

This linear expression was fitted to the $M_c$, $\chi_c$ data in the $20 < T < 80$ °K range using only $\alpha_0$ and $(D_1\alpha_0 + D_2)'$ as adjustable parameters. Data taken at higher temperatures were not used, as (27a) is a poor approximation to $\mu$ in this range.[20,35] The best fit to (30) was obtained for

$$\alpha_0 = -60 \pm 20 \text{ mrad}, \qquad (D_1\alpha_0 + D_2)' = 1.3 \pm 0.1 \text{ mole Oe/emu} . \quad (29b)$$

For $T/T_N < 0.4$, $\langle S \rangle \simeq S$, and (24a) can be written as

$$\Delta E_\alpha(T) = Ng_z'\mu_B^2 S(D_1\alpha_0 + D_2)' + \tfrac{1}{2}N(g_z')^2\mu_B^2 G_\alpha' \tanh\left(\frac{\Delta E_\alpha(T)}{2k_BT}\right) . \quad (31)$$

Thus we may regard $\Delta E_\alpha$ as a linear function of $\tanh(\Delta E_\alpha/2k_BT)$ with two adjustable parameters $g_z'(D_1\alpha_0 + D_2)'$ and $(g_z')^2 G_\alpha'$. Taking $g_z' = 11.3$, the best fit to (31) in the temperature range $4.2 < T < 50$ °K was obtained with

$$(D_1\alpha_0 + D_2)' = 1.4 \pm 0.1 \text{ mole Oe/emu}, \qquad G_\alpha' = 0.13 \pm 0.03 \text{ mole Oe/emu} . \quad (29c)$$

Finally, we analyzed the values of $g_z''$ obtained from the field-dependent optical data using (28). The reduced data and best two-parameter $(g_z', G_\alpha')$ linear fit are given in Fig. 13. The strong temperature dependence of the measured splitting factor is clearly evident. The fit shown was obtained with

$$g_z' = 11.2 \pm 0.3, \quad G_\alpha' = 0.11 \pm 0.04 \text{ mole Oe/emu} . \quad (29d)$$

Summarizing, the best values for the parameters given in (29a)–(29d) are

$$\alpha_0 = -60 \pm 20 \text{ mrad}, \quad g_z' = 11.3 \pm 0.3, \quad (D_1\alpha_0 + D_2)' = 1.4 \pm 0.1 \text{ mole Oe/emu}, \quad G_\alpha' = 0.13 \pm 0.03 \text{ mole Oe/emu} . \quad (32)$$

### B. $\Gamma_1$ phase

The $\Gamma_1$ or $\beta$ phase resembles the $\Gamma_4$ phase in that the effective field acting on an $Er^{3+}$ ion is along the $c$ crystallographic axis.[12] The Cr-Cr interaction Hamiltonian $\mathcal{H}_\beta^{\mathrm{Cr\text{-}Cr}}$, in the absence of an external field, is simply

$$\mathcal{H}_\beta^{\mathrm{Cr\text{-}Cr}} = -(\tfrac{1}{2}Ng_b\mu_B)^2\lambda S_{1y}S_{2y} , \quad (33)$$

$\lambda$ here being identical with the same coefficient in (2) as the Cr-Cr Heisenberg exchange interaction is isotropic. The $y$ axis $g$ factor is $g_b = 2$. In the $\Gamma_1$ phase, all $Er^{3+}$ moments are parallel or antiparallel to the $z$ direction, so $\mathcal{H}_\beta^{\mathrm{Er\text{-}Er}}$ is identical with $\mathcal{H}_\alpha^{\mathrm{Er\text{-}Er}}$ as given in (3) with $H_c = 0$. Since, however, the $Er^{3+}$ moments are in a $c_z$ mode in $\Gamma_1$, we here have

$$\langle J_{1z}\rangle = \langle J_{2z}\rangle = -\langle J_{3z}\rangle = -\langle J_{4z}\rangle . \quad (34)$$

Finally, the Cr-Er coupling in the $\Gamma_1$ phase is completely antisymmetric, and $\beta^{\mathrm{Cr\text{-}Er}}$ is given by

$$\mathcal{H}_\beta^{\mathrm{Cr\text{-}Er}} = (\tfrac{1}{4}N\mu_B)^2 g_b g_z D_3(J_{1z} + J_{2z} - J_{3z} - J_{4z})(S_{1y} - S_{2y}) . \quad (35)$$

The only experimental quantity of interest is the ground doublet splitting $\Delta E_\beta$ and, using (3) and (33)–(35), we obtain

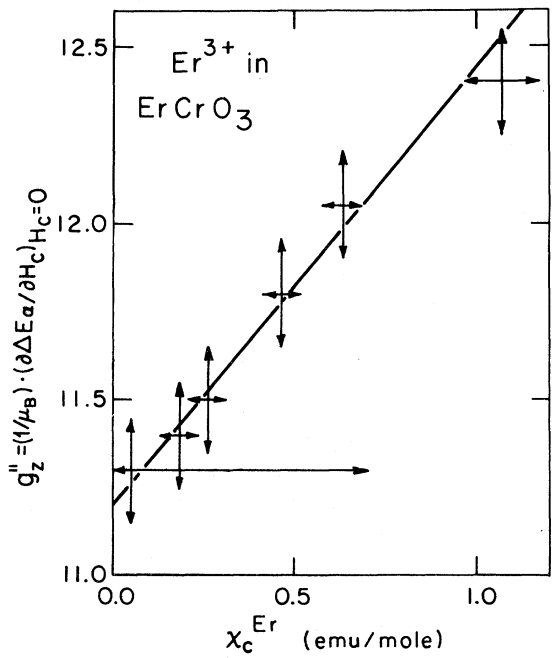


FIG. 13. Effective optical splitting factor $g_z''$ as a function of the susceptibility $\chi_c^{\mathrm{Er}}$ (see text).

$$\Delta E_\beta(T) = g_z \mu_B D_3 \mu + \tfrac{1}{2} N g_z^2 \mu_B^2 G_\beta \tanh[\Delta E_\beta(T)/2k_B T] , \tag{36}$$

with

$$G_\beta = G_1 + G_2 - G_3 - G_4 . \tag{37}$$

The coefficients $G_i$ are the same as those given in (3). Note that in (36) the quantities $g_z$ and $G_\beta$ are *not* renormalized.

Equation (36), of course, only applies when $4.2\ ^\circ\mathrm{K} < T < T_R$. In this temperature range $\mu$ is constant and equal to $\frac{3}{2}\mu_B N$. Regarding $\Delta E_\beta$ as a linear function of $\tanh(\Delta E_\beta/2k_B T)$, the best two-parameter fit to the experimental data was obtained with

$$\begin{aligned} g_z D_3 &= 16.9 \pm 1.2 \text{ mole Oe/emu} , \\ g_z^2 G_\beta &= 20.2 \pm 3.2 \text{ mole Oe/emu} . \end{aligned} \tag{38}$$

The theoretical curve obtained with these parameter values is shown in Fig. 6.

### C. $\Gamma_2$ phase

An analysis of the $\Gamma_2$- or $\gamma$-phase data is in principle much more difficult than for the other two phases. This is a consequence of the large number of independent coupling coefficients allowed by symmetry for this phase. In addition, low-temperature ($T < 15\ ^\circ\mathrm{K}$) optical absorption data are unavailable. We have therefore restricted our quantitative analysis of the $\Gamma_2$-phase data to temperatures greater than $20\ ^\circ\mathrm{K}$, where Er-Er interaction terms will have a minimal influence. We further assume that the canting angle is temperature independent, and that the dominant $Er^{3+}$ contribution to the magnetization and susceptibility is from electrons occupying the lowest-lying Kramers doublet. The constant-canting-angle assumption will be justified in Sec. IV. The equations appropriate to this model have been given elsewhere,[31] and we therefore present only the results:

$$\Delta E_\gamma(H_a, T) = \mu_B [g_\xi^2 (H_{\gamma 1} \cos\theta + H_a \cos\phi)^2 + g_\eta^2 (H_{\gamma 1} \sin\theta - H_a \sin\phi)^2]^{1/2} , \tag{39a}$$

$$M_a(T) = \pm 2\mu |\alpha_0| + m_a = \pm 2\mu |\alpha_0| \pm \tfrac{1}{2} N \bar{g} \mu_B \tanh\left(\frac{\Delta E_\gamma(T)}{2k_B T}\right), \tag{39b}$$

$$\chi_a(T) = \frac{1}{\lambda} + \frac{N\bar{g}^2 \mu_B^2}{4k_B T} \operatorname{sech}^2\left(\frac{\Delta E_\gamma(T)}{2k_B T}\right) + \frac{N\mu_B^2 (g_x^2 - \bar{g}^2)}{2\Delta E_\gamma(T)} \tanh\left(\frac{\Delta E_\gamma(T)}{2k_B T}\right) . \tag{39c}$$

In (39), $g_\xi$ and $g_\eta$ denote the in-plane components of the $Er^{3+}$ $g$ tensor in the principal axis system shown in Fig. 14, $H_{\gamma 1}$ is the magnitude of the effective field at each $Er^{3+}$ site due to the ordered $Cr^{3+}$ spins, and $H_a$ is the magnitude of the $a$-direction applied field. The angles $\theta$, $\phi$ are defined in Fig. 14, and $g_x$, $\bar{g}$ are given by

$$g_x = (g_\xi^2 \cos^2\phi + g_\eta^2 \sin^2\phi)^{1/2} , \tag{40a}$$

$$\bar{g} = \frac{|g_\xi^2 \cos\theta\cos\phi - g_\eta^2 \sin\theta\sin\phi|}{(g_\xi^2 \cos^2\theta + g_\eta^2 \sin^2\theta)^{1/2}} . \tag{40b}$$

The ground doublet splitting $\Delta E_\gamma(H_a, T)$ can also be written in the form

$$\Delta E_\gamma(H_a, T) = \{[\Delta E_\gamma(T)]^2 + 2\mu_B \bar{g} H_a \Delta E_\gamma(T) + \mu_B^2 g_x^2 H_a^2\}^{1/2} , \tag{41a}$$

where $\Delta E_\gamma(T)$, the extrapolated-to-zero-field splitting, is given by

$$\Delta E_\gamma(T) = \mu_B (g_\xi^2 \cos^2\theta + g_\eta^2 \sin^2\theta)^{1/2} H_{\gamma 1} = \mu_B g_\gamma H_{\gamma 1} . \tag{41b}$$

Since $H_{\gamma 1}$ in (39) and (41) is due only to the Cr-Er coupling, it follows that, in a single-ion constant-canting-angle model, it is given by

$$H_{\gamma 1} = \bar{D}\mu , \tag{42}$$

where $\bar{D}$ is an average coupling coefficient. In (39b) we have taken the magnitudes of the canting angles in the $\Gamma_2$ and $\Gamma_4$ phases to be equal. This is in accord with our earlier assumption that the Dzyaloshinsky interaction is the mechanism pri-

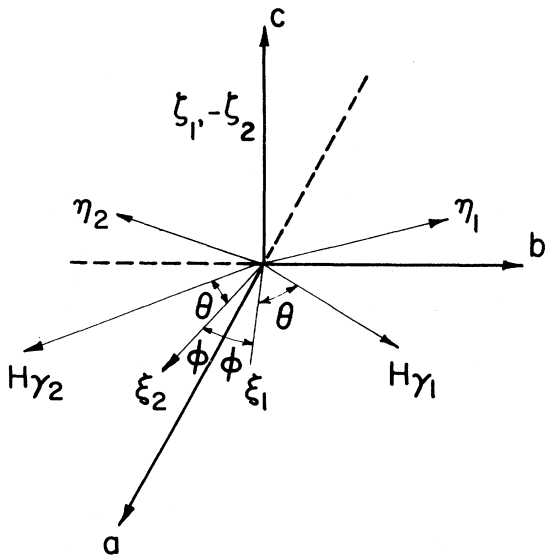


FIG. 14. Local principal magnetic axis ($\xi_i, \eta_i, \zeta_i$) for two inequivalent $Er^{3+}$ sites in $ErCrO_3$ and effective fields $H_\gamma$ in the $\Gamma_2(F_x)$ phase.

marily responsible for the canting. The plus or minus sign is to be assigned according to whether the Cr and Er contributions to $M_a$ are parallel or antiparallel.

In analyzing the experimental results, we first fitted (41) to the optical data shown in Fig. 7. The quantities $\bar{D}g_\gamma$, $\bar{g}$, and $g_x$ were treated as parameters, and a best fit was obtained for

$$\begin{aligned} &\bar{D}g_\gamma = 11.3 \pm 1.1 \text{ mole Oe/emu}, \\ &\bar{g} = 0.4 \pm 2.0, \\ &g_x = 5.9 \pm 0.6. \end{aligned} \tag{43}$$

Using parameter values within the error limits quoted in (43), (39b) could be satisfactorally fitted to the data for $M_a$. It was, however, not possible to obtain simultaneously a satisfactory fit to the $\chi_a$ data. This could be done by adding to (39c) a Van Vleck type susceptibility term[36]

$$\chi_a^{VV} = (|P|^2/\delta)\tanh(\delta/2k_BT). \tag{44}$$

Here, $\delta$ is the crystal-field splitting between the ground doublet and that elevated doublet of $^4I_{15/2}$ which dominates the Van Vleck contribution to $\chi_a$, and $P$ is the off-diagonal matrix element connecting these two doublets. Restricting ourselves to $\delta$ values given in Table I, a best fit was obtained for 166 °K, i.e., by a Van Vleck contribution caused by the mixing of the crystal-field doublets I and III by $H_{\gamma 1}$. Our final fit to all the experimental data for the $\Gamma_2$ phase is shown in Figs. 7, 11, and 12, and was obtained with the parameter values

$$\begin{aligned} &\bar{D}g = 11.3 \pm 1.1 \text{ mole Oe/emu}, \\ &\bar{g} = 2.0 \pm 0.5, \\ &g_x = 5.9 \pm 0.6, \\ &|P|^2/\delta = 0.1 \pm 0.02 \text{ mole Oe/emu}. \end{aligned} \tag{45}$$

(Note that while Van Vleck terms in principle contribute also to $\chi_c$, they would there be of less importance, as $\chi_c$ is considerably larger than $\chi_a$.) We see that, while the fit is generally excellent for $T > 15$ °K, the extension of (39b) and (39c) to lower temperatures does not give a satisfactory fit to the measured magnetization and susceptibility. We shall discuss reasons for this in Sec. IV.

## IV. DISCUSSION

In our analysis of the optical and magnetic data for $\Gamma_4$-phase $ErCrO_3$, we obtained the renormalized Er-Er coupling coefficient $G'_\alpha$. However, in order to know to what extent the back-reaction mechanism contributes to this quantity, an independent determination of $G_\alpha$ is necessary. In principle, $G_\alpha$ is due to a combination of exchange and dipole-dipole interactions between the $Er^{3+}$ magnetic moments. Of these, the dipole-dipole contribution can be evaluated directly. Since all our data are corrected to disk-shaped samples with the spontaneous magnetization lying in the disk plane, the appropriate demagnetizing factor is zero, and we need include in our calculation only a dipole sum over a spherical sample and a Lorentz term. Taking the necessary crystallographic parameters from the literature[2] and using standard techniques, we obtain

$$G_\alpha^{dip} = 0.17 \text{ mole Oe/emu}. \tag{46}$$

If the exchange contribution to the Er-Er interaction is negligible, (26c) requires that $G'_\alpha \geq G^{dip}$, with the equality holding only when $D_1/2\lambda \ll \sqrt{G_\alpha/\lambda} = 0.03$. Thus, $D_1 \ll 9$ mole Oe/emu, and $D_1\alpha_0 \ll 0.6$ mole Oe/emu. Comparing (32) with (46) and taking the probable error into consideration, we see that $G'_\alpha \simeq G_\alpha^{dip}$. It then follows from (26b) and (32) that the antisymmetric coupling term in (4) dominates the Cr-Er interaction.

Returning to the exchange contribution to $G'_\alpha$, we can estimate its importance by considering the $\Gamma_1$ phase. Here only the dipole sum term contributes to the dipole-dipole interaction, and direct calculation gives

$$G_\beta^{dip} = 0.16 \text{ mole Oe/emu}. \tag{47}$$

If the exchange contribution to $G_\alpha$ is indeed negligible, it follows from (26a) that $g_z = g'_z$. Under these conditions (38) yields $G_\beta = 0.16 \pm 0.03 = G_\beta^{dip}$. Thus our results, while they do not absolutely rule out exchange contributions to $G_\alpha$ and $G_\beta$, are consistent with the following conclusions: (i) The Er-Er interaction is predominantly of dipolar origin. (ii) The Cr-Er coupling in the $\Gamma_4$ phase is predominantly antisymmetric in nature. A direct calculation shows that the dipolar contribution to this interaction is small, indicating that an antisymmetric (Dzyaloshinsky-Moriya) exchange mechanism is responsible for the coupling. The same conclusion as to the Cr-Er antisymmetric coupling mechanism is reached for the $\Gamma_1$ phase after a dipole calculation.

Conclusion (i) is also supported by studies of Er-Er interactions in the isomorphic compounds $ErAlO_3$ and $ErFeO_3$. In $ErAlO_3$, the $Er^{3+}$ spin system orders antiferromagnetically at 0.6 °K in a $c_z$ mode. This spin structure is consistent with a dipolar origin for the Er-Er interaction.[37] In $ErFeO_3$, Mössbauer[38] and optical[22] studies have shown that the $Er^{3+}$ spin system orders cooperatively at 4.3 °K, again in a $c_z$ mode. Here also, the dipolar interaction was shown to account for the observed ground doublet splitting, indicating that Er-Er exchange coupling is negligible.[22,38]

However, recent work[39,40] has shown that a continuous spin reorientation of the $Fe^{3+}$ spin system occurs for $T<4.3$ °K, and the influence of this reorientation on the $Er^{3+}$ moments should also be considered when analyzing the low-temperature behavior of $Er^{3+}$ in $ErFeO_3$.

Conclusion (ii) leads immediately to the following values for $g_z$ and the coupling coefficients:

$$\begin{aligned} &g_z = 11.3 \pm 0.3, \\ &D_2 = 1.4 \pm 0.1 \text{ mole Oe/emu}, \\ &G_\alpha = 0.13 \pm 0.03 \text{ mole Oe/emu}, \\ &G_\beta = 0.16 \pm 0.03 \text{ mole Oe/emu}. \end{aligned} \tag{48}$$

For convenience in comparing these results with those reported elsewhere, the various effective fields and optical splittings obtained from these values are listed in Table III. Further, since $D_1 \ll 9$ mole Oe/emu, we see from (17) that the $\Gamma_4$-phase canting angle in zero applied field is equal to $\alpha_0$ and is temperature independent. As the basic nature of the Cr-Er coupling is expected to be the same in the $\Gamma_4$ and $\Gamma_2$ phases, this then justifies our taking $\alpha$ to be temperature independent in the $\Gamma_2$-phase data analysis in Sec. III C. A calculation of the dipolar part of the Cr-Er interaction in the $\Gamma_2$ phase shows that here also the coupling is predominantly of exchange origin.

From the discontinuity in the ground doublet splitting at $T_R$, the difference in the anisotropy energy $\Delta K$ of the $Cr^{3+}$ spin system in the two phases can be calculated. The spin reorientation takes place at constant (zero) external field and temperature, with no apparent hysteresis; thus the magnetic analog of the Gibbs free energy

$$F = F(\vec{H}, T) = \epsilon - T\sigma = \langle \mathcal{H} \rangle - T\sigma, \tag{49}$$

is continuous at the phase transition.

For the $\Gamma_4$ phase,

$$\begin{aligned} F_\alpha = &-\tfrac{9}{4}(\mu_B N)^2 \lambda - \tfrac{9}{8}(\mu_B N)^2 D^2/\lambda - K_\alpha \\ &- Nk_B T_R \ln\{2\cosh[\Delta E_\alpha(T_R)/2k_B T_R]\} \\ &+ \tfrac{1}{4} N \Delta E_\alpha^{Er}(0\,°\text{K}) \tanh^2[\Delta E_\alpha(T_R)/2k_B T], \end{aligned} \tag{50a}$$

where we have set $\langle S \rangle = S$ at $T = T_R$ and have evaluated the Er contribution to $E_\alpha$ directly from the partition function. [The final term in (50a) is to compensate for the usual double counting in the molecular-field approximation.[8]] Similarly, for the $\Gamma_1$ phase,

$$\begin{aligned} F_\beta = &-\tfrac{9}{4}(\mu_B N)^2 \lambda - K_\beta \\ &- Nk_B T_R \ln\{2\cosh[\Delta E_\beta(T_R)/2k_B T_R]\} \\ &+ \tfrac{1}{4} N \Delta E_\beta^{Er}(0\,°\text{K}) \tanh^2[\Delta E_\beta(T_R)/2k_B T_R]. \end{aligned} \tag{50b}$$

Setting $F_\alpha = F_\beta$ in (50), and taking $\lambda = 142$ mole Oe/emu, $D = 17$ mole Oe/emu, $T_R = 9.3$ °K, $\Delta E_\beta(T_R)/k_B = 10.4$ °K, $\Delta E_\beta(T_R)/k_B = 11.6$ °K, and $\Delta E_\alpha^{Er}(0\,°\text{K})$, $\Delta E_\beta^{Er}(0\,°\text{K})$ from Table III, we obtain

$$\Delta K/Nk_B = (K_\alpha - K_\beta)/Nk_B = (-0.57 \pm 0.15)\ °\text{K/spin} \tag{51}$$

for the difference between the $\Gamma_4$ and $\Gamma_1$ phase anisotropy energies at $T = T_R$.

Similarly, we can calculate the latent heat $T_R \Delta\sigma = NT_R(\Delta\sigma_S + \Delta\sigma_J)$, associated with the $\Gamma_4 \rightleftharpoons \Gamma_1$ spin reorientation. As $\Delta\sigma_S = 0$, we need consider only the entropy change due to the Er spin system. In the absence of an external field, we then have

$$T_R \Delta\sigma = \Delta\epsilon^{Er} - \Delta F^{Er} = \Delta\langle \mathcal{H}^{Er\text{-}Er} + \mathcal{H}^{Cr\text{-}Er} \rangle - \Delta F^{Er}, \tag{52}$$

where $\Delta E^{Er}$ and $\Delta F^{Er}$ are, respectively, the differences in the magnetic enthalpy and free energy of the $Er^{3+}$ spin system in the two phases. Using (3), (4), (35), and the appropriate part of (50), we obtain

$$\begin{aligned} T_R \Delta\sigma = &Nk_B T_R \left[ \ln\left( \frac{\cosh[\Delta E_\alpha(T_R)/2k_B T_R]}{\cosh[\Delta E_\beta(T_R)/2k_B T_R]} \right) \right] \\ &- \tfrac{1}{2} N \Delta E_\alpha(T_R) \tanh[\Delta E_\alpha(T_R)/2k_B T_R] \\ &+ \tfrac{1}{2} N \Delta E_\beta(T_R) \tanh[\Delta E_\beta(T_R)/2k_B T_R], \end{aligned} \tag{53a}$$

$$T_R \Delta\sigma/Nk_B = (0.25 \pm 0.05)\ °\text{K/spin}. \tag{53b}$$

This is in good agreement with the value of 0.2 °K/spin obtained directly from specific-heat measurements.[6]

Turning to the $\Gamma_2$ phase, the analysis we presented in Sec. III C was based on a model applicable only to the temperature region above approximately 20 °K, where the influence of the Er-Er interaction is minimal. As seen in Figs. 11 and 12, extending this model to lower temperatures results in magnetization and susceptibility values significantly different from those found experimentally. To obtain at least a qualitative explanation for this low-temperature behavior, we note

TABLE III. Calculated $Er^{3+}$ ground doublet splittings and effective fields at $Er^{3+}$ sites due to Cr-Er and Er-Er interactions. The values given are for zero applied field at 0 °K.

| Phase | Ground doublet splitting (in °K) due to Cr-Er | Ground doublet splitting (in °K) due to Er-Er | Effective field (in kOe) due to Cr-Er | Effective field (in kOe) due to Er-Er |
|---|---|---|---|---|
| $\Gamma_1(0)$ | 9.6 ± 0.6 | 3.8 ± 0.6 | 12.6 ± 1.3 | 5.0 ± 1.2 |
| $\Gamma_2(F_x)$ | 6.4 ± 0.6 | ... | ... | ... |
| $\Gamma_4(F_z)$ | 8.9 ± 0.6 | 3.1 ± 0.6 | 11.7 ± 0.8 | 4.1 ± 1.1 |

that in the $\Gamma_2$ phase the $Er^{3+}$ spins are in a $f_x c_y$ mode.[12] In a molecular-field framework, the Er-Er interaction can be written in the form[21,24]

$$\langle \mathcal{H}^{Er-Er} \rangle = -\tfrac{1}{2} G_{\gamma 1} m_a^2 - \tfrac{1}{2} G_{\gamma 2} m_b^2 - G_{\gamma 3} m_a m_b , \quad (54)$$

where

$$m_a = \tfrac{1}{2} g_x \mu_B N \langle J \rangle , \quad m_b = \tfrac{1}{2} g_y \mu_B N \langle J \rangle \quad (55)$$

are, respectively, the components of the $Er^{3+}$ sublattice moment along the $a$ and $b$ crystallographic axes. The effective $g$ factor $g_x$ was defined earlier in (40a), and $g_y$ is given by

$$g_y = (g_\xi^2 \sin^2\phi + g_\eta^2 \cos^2\phi)^{1/2} . \quad (56)$$

If we assume that the $\Gamma_2$ Er-Er coupling is also of dipolar origin, the three interaction constants $G_{\gamma i}$ can be calculated directly. Using the method described at the beginning of this section, one obtains

$$G_{\gamma 1} = 0.19, \quad G_{\gamma 2} = -0.18, \quad G_{\gamma 3} = 0.027 \text{ mole Oe/emu.} \quad (57)$$

The results of the dipolar calculation show that $H_\gamma^{Er-Er}$ will increase $M_\alpha(T)$ above the value obtained with $H_{\gamma 1}$ alone. This is clear from (57), which shows that the dipolar coupling favors $f_x$ over $c_y$ for the $Er^{3+}$ $\Gamma_2$-phase spin structure. The resulting increase in $M_a(T)$ is thus not due only to an increase in the magnitude $H_\gamma$ of the effective field, but also to a change in the angle $\theta$ between $\vec{H}_\gamma$ and the $\xi$ axis. This change in $\theta$ will be reflected in an increase in the effective $g$-factor $\bar{g}$ appearing in (39b), and in a corresponding increase in $M_a(T)$. In addition, although the expression for $\chi_a(T)$ given by (39c) is no longer completely adequate in the presence of Er-Er coupling, we see that an increase in $g$ will increase the coefficient of the $\mathrm{sech}^2[\Delta E_\gamma(T)/2k_BT]$ term and reduce that of $\tanh[\Delta E_\gamma(T)/2k_BT]$. This shift in the relative contributions of these two terms could then result in a peak in $\chi_a(T)$ at low temperatures.

We thus see that adding to the $\Gamma_2$ phase Hamiltonian an Er-Er coupling term of dipolar origin could explain the low-temperature behavior of the magnetization and $a$-axis susceptibility. However, in view of the large number of unknown coefficients and the lack of $\Gamma_2$-phase optical-absorption data below $T = 15\,^\circ$K, we did not feel that a full quantitative analysis was justified.

A summary of our results for $ErCrO_3$ in the $\Gamma_1$, $\Gamma_2$, and $\Gamma_4$ phases is given in Table IV. In addition, we give the corresponding values found in other studies and also the results of similar studies on $ErFeO_3$. In general we see that the results for the crystal-field properties of the orthochromite and orthoferrite are quite similar. In addition, for both compounds, the Cr-Er coupling is essentially due to antisymmetric exchange,[41] while the Er-Er interaction is dipolar.[22,38]

A comprehensive theory of spin-reorientation phase transitions in the rare-earth orthochromites and orthoferrites has been given recently by Yamaguchi.[42] His treatment differs from ours in several respects, the most important of which is that Yagamuchi does not include in his Hamiltonian rare-earth–rare-earth coupling terms. The justification for this is that these are expected to be small compared with transition-metal–transition-metal and transition-metal–rare-earth coupling terms. However, it is clear that the quantities that enter into the spin-reorientation process are the *differences* in the *magnitudes* of the various free-energy contributions in the initial and final phases. In the case of $ErCrO_3$, for example, it is the difference in the contribution of the Cr-Er term to the free energy in the $\Gamma_4$ and $\Gamma_1$ phases that should be compared with the difference in the Er-Er free-energy contribution. On this basis, our results show that Er-Er coupling is not negligible. In fact (see Tables III and IV), the Cr-Er and Er-Er contributions to the abrupt change in the ground doublet splitting at the spin-reorientation temperature are approximately equal. Since Yamaguchi's model emphasizes the role of transition-metal–rare-earth coupling in a spin-reorientation process, this model is most suited to the study of reorientations that occur at higher temperatures, where the rare-earth–rare-earth contribution will indeed be of minor importance.

Another recent study of magnetic interactions in the orthochromites is that of Cooke *et al.* on $GdCrO_3$.[43] This compound exhibits a spontaneous spin reorientation between the $\Gamma_2$ and $\Gamma_4$ phases. Cooke *et al.* find that the Cr-Gd coupling is anisotropic with effective fields of 5.5 and 6.4 kOe for the $\Gamma_2$ and $\Gamma_4$ phases, respectively. Note that the anisotropy in the effective field is of the same order as that found between the $\Gamma_1$ and $\Gamma_4$ phases of $ErCrO_3$ (see Table III).

Finally, we note the work of Walling and White[44] on $HoFeO_3$. These authors also conclude that the transition-metal–rare-earth coupling is predominantly due to antisymmetric exchange, and that the rare-earth–rare-earth coupling is not negligible at temperatures below 30 °K.

In conclusion, by means of combined absorption-spectroscopy and bulk-magnetization measurements, the magnetic properties of $ErCrO_3$ have been studied as a function of temperature and external field. We have found that these properties can be understood in terms of a single-ion model which treats the interactions between the electrons occupying the lowest-lying Kramers doublet of the $Er^{3+}$ ion and the $Cr^{3+}$ and $Er^{3+}$ spin systems by

TABLE IV. Comparison of $ErCrO_3$ with $ErFeO_3$. [$T_R$ — $\Gamma_4(F_z) \rightleftarrows \Gamma_1(0)$ spin-reorientation temperature; $g_z$, $g_x$ — effective $g$ factors of $Er^{3+}$ along the $c$ and $a$ axes; $\alpha_0$ — canting angle of the $Cr^{3+}$ spin system; $\Delta E_\alpha(T)$, $\Delta E_\beta(T)$ — $Er^{3+}$ ground-doublet splittings in the $\Gamma_4(F_z)$ and $\Gamma_1(0)$ phases, respectively, at temperature $T$; $\Delta K$— difference in anisotropy energy of $\Gamma_4(F_z)$ and $\Gamma_1(0)$ phases at $T = T_R$; $T_R \Delta\sigma$ — latent heat associated with $\Gamma_4(F_z) \rightleftarrows \Gamma_1(0)$ spin reorientation; $E_{II}$, $E_{III}$, $E_{IV}$, $E_V$ — crystal-field splittings between ground Kramers doublet and first four elevated doublets.]

| | $ErCrO_3$ [a] | $ErCrO_3$ [b] | $ErCrO_3$ [c-e] | $ErCrO_3$ [f] | $ErCrO_3$ [g] | $ErCrO_3$ [h] | $ErFeO_3$ [i, j] | $ErFeO_3$ [k] | $ErFeO_3$ [l] |
|---|---|---|---|---|---|---|---|---|---|
| $T_R$ (°K) | 9.3 ± 0.5 | 9.4 ± 0.5 | 9.82 ± 0.02 [c] | 9 ± 1 | 9 ± 1 | | | | |
| $g_z$ | 11.3 ± 0.3 | 11.1 ± 0.9 | 10.4 [d] | 12.2 | 11.6 ± 0.8 | 12.4 | 11.5 [i] | 13.2 ± 4 | 13.1 ± 0.4 |
| $g_x$ | 5.9 ± 0.6 | | | | | | 6 [i] | | |
| $\alpha_0$ (mrad) | −60 ± 20 | | −35 [e] | | | | 8 [j] | | |
| $\Delta E_\alpha(T)$ (°K) | 10.3 (9.3 °K) ± 0.2 | 10.2 (9.7 °K) ± 0.2 | | | 10.1 (10 °K) | 10 (10 °K) | | | |
| $\Delta E_\beta(T)$ (°K) | 11.6 (9.3 °K) ± 0.2 | 11.6 (9.0 °K) ± 0.2 | 13.5 ($T < T_R$) [c] | 12 ($T < T_R$) | 13.2 (4.2 °K) | 15 (4.2 °K) | | | 9.2 (0 °K) ± 0.6 |
| $\Delta K/Nk_B$ (°K/formula unit) | −0.57 ± 0.15 | −0.45 ± 0.08 | −0.45 [d] | ≃−1 | | | | | |
| $T_R \Delta\sigma/Nk_B$ (°K/formula unit) | 0.25 ± 0.05 | 0.15 ± 0.05 | 0.2 [c] | | | | | | |
| $E_{II}$ (°K) | 66 ± 1 | 66 ± 1 | | | | | 66 [i] | 66 | |
| $E_{III}$ (°K) | 164 ± 3 | 162 ± 2 | | | | | 157 [i] | 160 | |
| $E_{IV}$ (°K) | | | | | | | 188 [i] | | |
| $E_V$ (°K) | 248 ± 4 | | | | | | 238 [i] | | |

[a] This work ($Er^{3+}$ optical-absorption-spectroscopy and single-crystal-magnetization studies).
[b] Ref. 8 ($Er^{3+}$ optical-absorption-spectroscopy studies).
[c] Ref. 6 (specific-heat studies).
[d] Ref. 2 (neutron-diffraction studies).
[e] Ref. 5 (single-crystal-magnetization studies).
[f] Ref. 3 (single-crystal-magnetization and powder specific-heat studies).
[g] Ref. 9 ($Cr^{3+}$–$Er^{3+}$ optical-absorption-spectroscopy studies).
[h] Ref. 7 (Mössbauer studies).
[i] Ref. 41 ($Er^{3+}$ optical-absorption-spectroscopy studies).
[j] Ref. 29 (single-crystal-magnetization studies).
[k] Ref. 22 ($Er^{3+}$ optical-absorption-spectroscopy studies).
[l] Ref. 38 (Mössbauer studies).

means of effective fields. For the $\Gamma_4$ and $\Gamma_1$ phases the most general coupling terms allowed by symmetry were considered, and the canting angle of the ordered $Cr^{3+}$ spins was not contrained *a priori* to be temperature independent. It was found that the Cr-Er coupling is antisymmetric in nature and due mainly to a Dzyaloshinsky-Moriya type exchange interaction. For this type of interaction, the $Cr^{3+}$ canting angle is indeed essentially temperature independent, and this conclusion therefore justifies the constant-canting-angle approximation used extensively in the literature.[15-17] The Er-Er coupling term was found to be of dipolar origin. It was shown that this interaction resulted in a significant temperature dependence of the effective splitting factor deduced from optical-absorption measurements. For the $\Gamma_2$ phase, both the optical-absorption and bulk-magnetization data for temperatures above 20 °K were interpreted in terms of a constant-canting-angle model for the Cr-Er interaction. At lower temperatures it was argued that the dipolar Er-Er coupling must also be considered.

ACKNOWLEDGMENTS

We are indebted to J. D. Gordon, Professor G. Gorodetsky, Dr. D. Mukamel, Professor S. Shtrikman, and Professor D. Treves for many helpful discussions and suggestions during the course of this work. The technical assistance of Y. Chopin, D. Leibovitz, and Y. Lipkin is gratefully acknowledged.

---

*Present address: Ministry of Defence, Scientific Department, Post Office Box 7063, Tel Aviv, Israel.
†To whom all reprint requests should be addressed.
‡Present address: High Power Laser Laboratory, Soreq Nuclear Research Center, Yavneh, Israel.
§Present address: Department of Physics, University of Manitoba, Winnipeg, Manitoba, Canada.

[1]S. Geller and E. A. Wood, Acta Crystallogr. 9, 563 (1956); S. Geller, J. Chem. Phys. 24, 1236 (1956); E. F. Bertaut and F. Forrat, J. Phys. (Paris) 17, 129 (1956).
[2]E. F. Bertaut and J. Mareschal, Solid State Commun. 5, 93 (1967).
[3]C. Veyret, J. B. Ayasse, J. Chaussy, J. Mareschal, and J. Sivardiere, J. Phys. (Paris) 31, 607 (1970).
[4]E. F. Bertaut, J. Mareschal, R. Pauthenet, and J. P. Rebouillat, Bull. Soc. Fr. Ceram. A 75, 44 (1966).
[5]L. Holmes, M. Eibschütz, and L. G. Van Uitert, J. Appl. Phys. 41, 1184 (1970).
[6]M. Eibschütz, L. Holmes, J. P. Maita, and L. G. Van Uitert, Solid State Commun. 8, 1815 (1970).
[7]M. Eibschütz, R. L. Cohen, and K. W. West, Phys. Rev. 178, 572 (1969).
[8]R. Courths, S. Hüfner, J. Pelzl, and L. G. Van Uitert, Solid State Commun. 8, 1163 (1970); Z. Phys. 249, 445 (1972).
[9]R. S. Meltzer and H. W. Moos, J. Appl. Phys. 44, 1240 (1970).
[10]R. S. Meltzer, Phys. Rev. B 2, 2398 (1970).
[11]W. C. Koehler, E. O. Wollan, and M. K. Wilkinson, Phys. Rev. 118, 58 (1960).
[12]E. F. Bertaut, in *Magnetism*, edited by G. T. Rado and H. Suhl (Academic, New York, 1963), Vol. III, p. 149.
[13]E. F. Bertaut, J. Mareschal, G. de Vries, R. Aléonard, R. Pauthenet, J. P. Rebouillat, and J. Sivardiere, IEEE Trans. Magn. 2, 453 (1966).
[14]R. L. White, J. Appl. Phys. 40, 1061 (1969).
[15]S. Shtrikman, B. M. Wanklyn, and I. Yaeger, Int. J. Magn. 1, 327 (1971).
[16]R. M. Hornreich, B. M. Wanklyn, and I. Yaeger, Int. J. Magn. 2, 77 (1972).
[17]R. M. Hornreich, B. M. Wanklyn, and I. Yaeger, Int. J. Magn. 4, 313 (1973).
[18]M. Eibschütz, Acta Crystallogr. 19, 337 (1965); P. Coppens and M. Eibschütz, *ibid.* 19, 524 (1965).
[19]A. Hasson, M.Sc. thesis (Technion, Israel Institute of Technology, Haifa, 1971) (unpublished).
[20]I. Yaeger, Ph.D. thesis (Weizmann Institute of Science, Rehovot, Israel, 1973) (unpublished).
[21]Y. Komet, Ph.D. thesis (Weizmann Institute of Science, Rehovot, Israel, 1974) (unpublished).
[22]R. Faulhaber, S. Hüfner, E. Orlich, and H. Schubert, Z. Phys. 204, 101 (1967).
[23]See, for example, M. Tinkham, *Group Theory and Quantum Mechanics* (McGraw-Hill, New York, 1965).
[24]A. P. Malozemoff, Technical report, Stanford Electronic Laboratories, Stanford, California, 1970 (unpublished).
[25]A. P. Malozemoff, J. Phys. Chem. Solids 32, 1669 (1971).
[26]G. Cinader and S. Shtrikman, Solid State Commun. 4, 459 (1966).
[27]T. J. Beaulieu, Report, Microwave Laboratory, Stanford University, Stanford, California, 1967 (unpublished).
[28]G. Gorodetsky, S. Shtrikman, Y. Tenenbaum, and D. Treves, Phys. Rev. 181, 823 (1969).
[29]D. Treves, J. Appl. Phys. 36, 1033 (1965); Phys. Rev. 125, 1843 (1963).
[30]I. S. Jacobs, H. F. Burne, and L. M. Levinson, J. Appl. Phys. 42, 1631 (1971).
[31]R. M. Hornreich and I. Yaeger, Int. J. Magn. 4, 71 (1973).
[32]G. H. Wannier, *Statistical Physics* (Wiley, New York, 1966), Chap. 8.
[33]H. Thomas, in Proceedings of the Chania International Conference on Magnetism, Crete, 1969 (Gordon and Breach, New York, to be published).
[34]G. Gorodetsky and D. Treves, in *Proceedings of the International Conference on Magnetism, Nottingham, 1964* (Institute of Physics and The Physical Society, London, 1965), p. 606.
[35]M. Eibschütz, S. Shtrikman, and D. Treves, Phys. Rev. 156, 562 (1967).
[36]J. H. Van Vleck, *The Theory of Electric and Magnetic Susceptibilities* (Oxford U. P., London, 1932), p. 232.

[37]J. Sivardiere and S. Quezel-Ambrunaz, C. R. Acad. Sci. (Paris) 273, 619 (1971).
[38]W. Wiedmann and W. Zinn, Z. Agnew. Phys. 20, 327 (1966).
[39]N. M. Kovtun, G. A. Troitskii, V. M. Khmara, and A. Ya. Chervonenkis, Zh. Eksp. Teor. Fiz. Pis'ma Red. 17, 277 (1973) [Sov. Phys.–JETP Lett. 17, 199 (1973)].
[40]G. Gorodetsky, R. M. Hornreich, I. Yaeger, H. Pinto, G. Shachar, and H. Shaked, Phys. Rev. B 8, 3398 (1973).
[41]D. L. Wood, L. M. Holmes, and J. P. Remeika, Phys. Rev. 185, 689 (1969).
[42]T. Yamaguchi, J. Phys. Chem. Solids 35, 479 (1974).
[43]A. H. Cooke, D. M. Martin, and M. R. Wells, J. Phys. C 7, 3133 (1974).
[44]J. C. Walling and R. L. White, Phys. Rev. B 10, 4748 (1974).